London Journal of PHYSICS

Volume 2 No 1

Remarkable Thermoelectric and Magnetic Properties of Anti-Perovskite $MgCNi_3$: A Pathway to Advanced Energy Conversion and Spintronics

Zahid Ullah[1,2*], Muhammad Amir Khan[1*], Sabahat Gul[1,2], Muhammad Noman[2], Salim Ullah[2], Murtaza Shahab[2]

[1]Faculty of Physical and Numerical Sciences, Qurtuba University of Science and Information Technology, Peshawar, Pakistan.
[2]Physics Department, Islamia College University, Peshawar, Pakistan.

*zuzohaad@gmail.com (Zahid Ullah),**makphy83@gmail.com (Muhammad Amir Khan).

May 27, 2025

Abstract

This study employs first-principles calculations based on density functional theory (DFT) with the GGA+U approximation to examine the structural, electronic, magnetic, and thermoelectric properties of $MgCNi_3$. The results reveal that $MgCNi_3$ is a weak ferromagnetic and metallic material, characterized by strong covalent bonding and a net magnetic moment of 0.15 μB per formula unit. Spin-polarized calculations further indicate that the material exhibits a non-zero magnetization, with the spin-up and spin-down electron densities showing distinct distributions. The thermoelectric evaluation demonstrates remarkable energy conversion efficiency, with a significant Seebeck coefficient and high figure of merit (ZT) across temperatures ranging from 300K to 900K. The ZT plot suggests that P-type doping may offer the best performance. These findings provide critical insights into the material's potential for applications in thermoelectrics, superconductors, and spintronics, emphasizing its suitability for integration into advanced functional devices.

1 Introduction

Anti-perovskite materials have emerged as promising candidates for the advancement of modern technologies due to their unique structural, electrical, and magnetic characteristics. Their relevance spans a wide spectrum of next-generation applications, including superconducting devices, spintronic memory systems, thermoelectric energy conversion, and energy storage capacitors [[1],[2]]. These materials have great potential for use in nanoscale devices and strain-engineered microelectronics, where excellent functional performance and high mechanical stability are crucial [[3],[4],[5],[6]]. The atomic arrangement of anti-perovskites (AX_3B) is inverted, with X being a cation and A and B being anions, in contrast to typical perovskites (AX_3B). Their unique structural arrangement allows for the fine-tuning of properties like spin-polarized conductivity, thermoelectric efficiency, and superconductivity, especially with transition metal elements like Ni. This makes them ideal for low-power electronics, high-performance computing, and quantum devices [4]. Anti-perovskites, such as $MgCNi_3$, are perceived as a novel class of quantum materials with enormous potential due to the continuous worldwide research being conducted on these materials.

The synthesis and structural stability of anti-perovskites provide substantial scientific restriction that limit their wider application, despite their promising qualities. According to published research, orbital hybridization, strain conditions, and lattice distortions, particularly those involving Ni's partially filled d-orbitals, that all affect the electrical and magnetic behavior of materials like $MgCNi_3$ and others. $MgCNi_3$ shows a cubic perovskite crystal structure with metallic bonding in experimental investigation [[7],[8],[9],[10]]. Consistent material performance is hampered, nevertheless, by instability under different temperature and

 DOI 10.69710/ljp.v2i1.14179

pressure settings as well as the challenge of preserving phase stability in thin films. Through the analysis of cohesive energies and phonon dispersions, computational studies have sought to overcome these restrictions and validate the dynamical and thermodynamic stability of $MgCNi_3$. In these investigations, it is found that the presence of substantially negative cohesive energy values and the lack of imaginary phonon modes indicate robustness against thermal and mechanical perturbations [7-9]. Still, there hasn't been a thorough investigation of these materials' thermoelectric qualities, despite tremendous theoretical and experimental advancements.

The lack of latest investigated research combining structural optimization, electron charge density mapping, and thermal transport modeling specifically for thermoelectric applications is the gap in the current body of knowledge. Despite the fact that superconducting and magnetic properties have been the subject of countless investigations, little is known about the thermoelectric behavior of $MgCNi_3$, particularly in thin-film topologies under various strain circumstances [[11],[12],[13]]. Systematic research on anti-perovskite materials is further constrained by regional issues, such as the scarcity of synthesis methods and experimental equipment in underdeveloped nations [[14],[15]]. Utilizing computational approaches offers a powerful and affordable tool for examining material properties in the setting of regional research institutes and materials science labs in nations like Pakistan. The development of optimal anti-perovskite compositions appropriate for energy applications in resource-constrained contexts can be greatly accelerated by the use of machine learning algorithms and first-principles calculations to forecast stability, bonding nature, and thermal performance.

In order to fill this research gap, the current study uses first-principles simulations to investigate the thermoelectric characteristics of $MgCNi_3$. The goals are to use cohesive energy and phonon dispersion methods to evaluate the structural, electronic, and dynamical stability; analyze charge density distributions to comprehend bonding characteristics; and examine trends in thermal conductivity to determine whether it is suitable for thermoelectric applications [[16],[17],[18],[19],[20],[21],[22]]. Investigating the thermoelectric characteristics of $MgCNi_3$ with an emphasis on comprehending how electronic interactions, atomic bonding, and strain modulation affect energy transport pathways is the ultimate goal of this work. This work aims to establish a strong basis for the creation of high-efficiency thermoelectric materials in the anti-perovskite family by coordinating theoretical predictions with experimental characteristics [[23],[24],[25],[26],[27],[28],[29]]. This work adds to the larger scientific effort of creating environmentally stable, energy-efficient materials for tomorrow's technology, paying special attention to the local research setting.

2 Method of Calculations

The structural, electronic, thermoelectric, and magnetic properties of $MgCNi_3$ were investigated using WIEN2k, a first-principles computational package grounded in density functional theory (DFT) and based on the full-potential linearized augmented plane wave (FP-LAPW) method [[30],[31],[32],[33],[34],[35],[36]]. This method uses first principles to solve the quantum mechanical equations driving electron interactions, allowing for high-precision structural and electronic structure calculations. Perdew and colleagues developed the generalized gradient approximation with Hubbard U correction (GGA+U) and the local density approximation (LDA) to precisely assess structural and electrical features as shown in Flow chart 1. Using the magnetic moment technique, which accurately depicts the spin-polarized behavior of electrons, magnetic properties were evaluated. The BoltzTraP code, which computes semi-classical transport coefficients based on the electronic structure derived from DFT, was used to investigate thermoelectric properties [32-36]. Essential thermoelectric parameters like the Seebeck coefficient, electrical conductivity, thermal conductivity, power factor, and figure of merit as functions of temperature and chemical potential are provided by BoltzTraP, which solves the Boltzmann transport equations under the constant relaxation time approximation [[37],[38],[39],[40]]. By forecasting how well $MgCNi_3$ can transform heat into electrical energy, these calculations provide important information about the material's potential for thermoelectric applications. By using these sophisticated computational methods, theoretical predictions become more accurate and more in line with experimental observations.

 DOI 10.69710/ljp.v2i1.14179

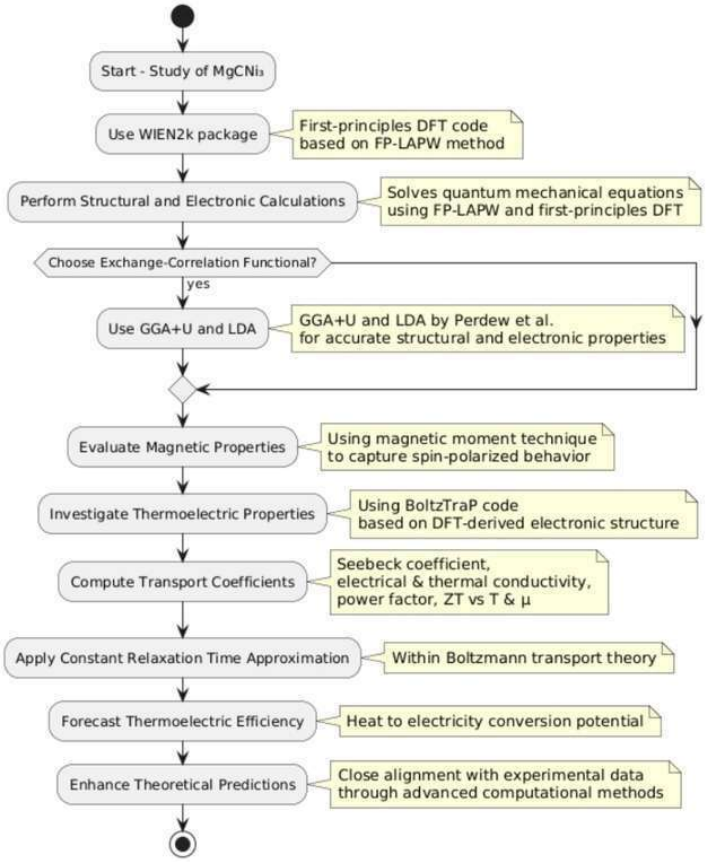

Flowchart 1. for studying structural, electronic, thermoelectric,and magnetic properties using spin-polarized DFT.

3 Results and Discussion

In this section, we explore various properties and characteristics of the material $MgCNi_3$ to understand its structural, electronic, thermoelectric and magnetic behavior in detail.

3.1 Structural Properties

The first-principles full-potential linearized augmented plane wave (FP-LAPW) approach has been used to analyze the structural characteristics of $MgCNi_3$ inverse perovskite within the framework of density functional theory (DFT) [[41],[42],[43]]. The GGA+U exchange-correlation functional was used to determine the equilibrium unit cell volume ($V_)$), bulk modulus (B), and its pressure derivative (B'). As atomic size increases, the bulk modulus of $CdCNi_3$ shows a trend of decreasing stiffness, confirming the expected inverse relationship between compressibility and lattice expansion. 5.000 was found to be the pressure derivative B' for $MgCNi_3$, indicating a stable mechanical response to pressure variations. These results highlight the importance of atomic size in affecting mechanical stability and support previous research on perovskite materials through computer analysis.The declining plot line in the structural optimization plot shows stability, indicating that the material has become more stable, as seen in Figure 1. With the theoretical and experimental lattice properties described in Table 1, the unit cell of the material under investigation displays a cubic inverse perovskite crystal structure, as shown in Figure 2.

Inverse perovskites, particularly those with carbon as the anion, have received little attention in previous research, which has mostly focused on conventional perovskites. The structural integrity of $MgCNi_3$ under ambient conditions is highlighted by its cubic phase stability in the Pm-3m space group. According to a comparison study with other $ACNi_3$ compounds, $CdCNi_3$ has mechanical qualities that fall between $ZnCNi_3$

 DOI 10.69710/ljp.v2i1.14179

and $MgCNi_3$, in line with trends in atomic radius. The mechanical properties of $CdCNi_3$ are influenced by a noticeable anion-cation inversion, which sets it apart from oxygen-based perovskites. By offering a thorough evaluation of their volumetric and mechanical characteristics, this work advances our understanding of inverse perovskites and advances the field of carbon-based perovskite materials.

The computational analysis of $MgCNi_3$ in this study is intriguing since it offers new information on its bulk modulus and pressure response. In order to provide a prediction framework for comparable materials, the study creatively correlated periodic atomic trends with macroscopic material features. Limitations do remain, though, mainly because of the absence of experimental confirmation and possible temperature-dependent effects that could change phase stability. Further research into $MgCNi_3$'s electrical and magnetic properties would also offer a more thorough understanding of its possible uses, even if its mechanical qualities have been well examined. Notwithstanding these difficulties, this research makes a substantial contribution to our understanding of inverse perovskites and establishes the foundation for their possible employment in technical applications in the future.

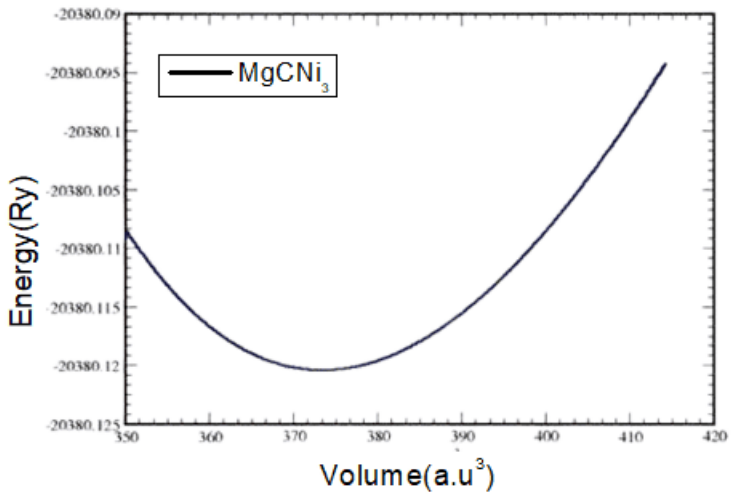

Figure 1: Cubic optimization plot of inverse perovskite $MgCNi_3$, showing the optimized atomic arrangement within the unit cell.

Table 1: Calculated lattice parameter (a in Å), bulk modulus (B in GPa), pressure derivative (B), unit cell volume (V in Å³), and ground state energies for $MgCNi_3$ inverse perovskite crystallized in the cubic (Pm-3m) phase for spin state (S) using the GGA potential.

Compound	**a_o(Å)**	**B(GPa)**	**B´**	**V_o(Å³)**	**E_o(eV)**
$MgCNi_3$					
Calculated(S)	3.81		5.000		-20380.1204
Experimental	3.84	210.9844		373.3923	

3.2 Electronic Charge Density

Understanding the bonding properties of materials requires knowledge of the electron charge density. It provides a thorough examination of electronic dispersion and clarifies whether a material's bonding is mostly

 DOI 10.69710/ljp.v2i1.14179

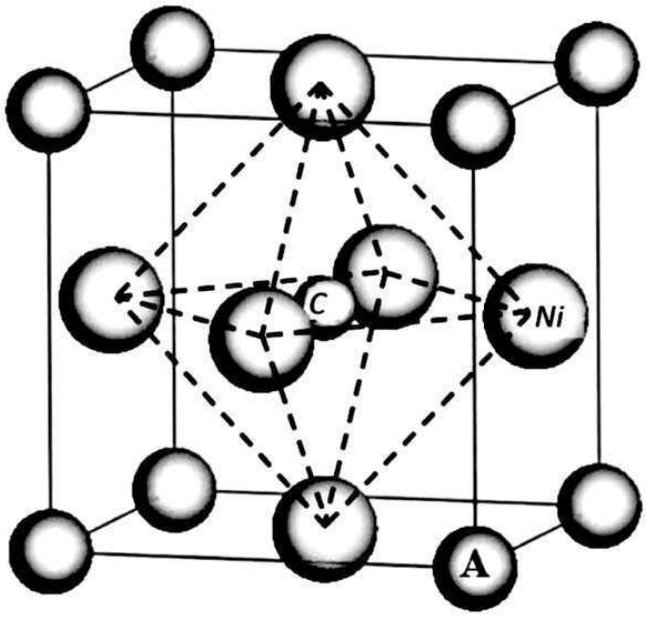

Figure 2: Cubic crystal structure of inverse perovskite $MgCNi_3$, illustrating the atomic arrangement and spatial configuration within the unit cell.

ionic or covalent. Charge density can be analyzed along certain crystallographic planes in density functional theory (DFT) calculations to clarify the nature of atomic interactions [[44],[45]]. Using electron charge density plots along the (100) plane, as shown in Figure 3, this work investigated the bonding properties of the inverse-perovskite MgCNi3. According to the study, $MgCNi_3$ bonding is primarily metallic, with significant covalent contributions in comparison to ionic bonding. Electrons are delocalized and not tightly confined to individual atoms, as shown by the charge density overlaps between nearby atoms. Electrons can move freely throughout the lattice due to the delocalization property of metallic bonds, which improves electrical conductivity. Since the electron density features are symmetrically distributed and show no discernible localization, the spin-polarized charge density emphasizes the metallic character. The results demonstrate $MgCNi_3$'s unique bonding properties, where the interplay of covalent and metallic forces amplifies its remarkable electrical and magnetic properties, establishing it as a potential contender for cutting-edge technological applications.

3.3 Band Structure

The Generalized Gradient Approximation (GGA+U) method inside density functional theory (DFT) was used to calculate the band structure of the inverse perovskite $MgCNi_3$ [[46],[47]]. Important information about this material's electrical characteristics is given in Figure 4. The metallic character of $MgCNi_3$ is confirmed by the Fermi energy level, which is 0.0 eV. This metallic conductivity is further supported by the overlapping of the electronic states at different symmetry sites, such as Γ, X, and R. Interestingly, the distinctive metallic behavior, where the conduction band is partially filled, is indicated by the junction of the valence band maxima with the conduction band minima at various symmetry positions. The compound's metallic nature is further emphasized by the significant overlap of states at the M symmetry point, which is seen in Figure 4. The general behavior is consistent with metallic conductivity, while certain symmetry points point to superconducting properties, such as overlapping conduction band states. One of the main reasons for $MgCNi_3$'s exceptional conductive qualities is the lack of a band gap. Because of its strong covalent bonding, weak ferromagnetism, and metallic conductivity, $MgCNi_3$ is a promising material for a variety of cutting-edge

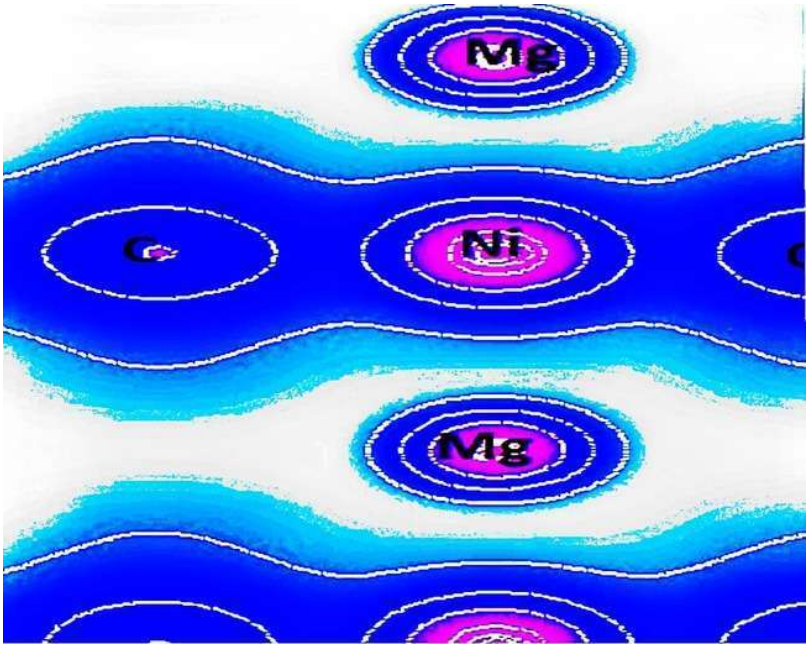

Figure 3: Electron charge density distribution of $MgCNi_3$ calculated using the GGA + U method.

electrical and magnetic applications, demonstrating its promise for future technological advancements.

3.4 Density of States

The electrical structure and bonding properties of the $MgCNi_3$ inverse perovskite are clarified by the density of states (DOS). Figure 5 shows the results of the density of states (DOS) calculations using the generalized gradient approximation (GGA + U) method in density functional theory (DFT). These curves help determine whether a material is a metal, non-metal, or semimetal. The partial density of states (PDOS) and total density of states (TDOS), which represent the frequency of electronic states in the valence and conduction bands, can be used to determine the band structure and electron density distribution [[48],[49]]. The partial density of states (PDOS) and total density of states (TDOS) plot for $MgCNi_3$ are shown in Figure 5, providing a thorough understanding of its electronic properties.

For $MgCNi_3$, the spin-polarized density of states (DOS) and projected density of states (PDOS) calculations fall between -8 eV and 7 eV. Mg-s, Ni-d, Ni-dxy, and Ni-dxy+dyz are the main contributors to the electronic states below the Fermi energy level, whereas Mg-p, Mg-d, C-p, and Ni-dz^2 show a comparatively less contribution. The Mg-s, Ni-d, and Ni-p orbitals have the most influence on the conduction band. Strong hybridization between these elements is indicated by the predominance of Ni and Mg states in the valence and conduction bands, which influences the electrical properties of the material.

The analysis of the electronic structure of $MgCNi_3$ confirms its metallic properties, as evidenced by the continuous Fermi-level density of states. $MgCNi_3$ has unique electrical characteristics in contrast to other $ACNi_3$ inverse perovskites, with Ni-d states having a major impact on its conductivity. Our understanding of the localization and interaction of electrons in this material is enhanced by the thorough examination of TDOS and PDOS, which facilitates potential applications in electronic and functional materials.

3.5 Seebeck Coefficient

The Seebeck coefficient of $MgCNi_3$ at temperature range 300K to 900K, graphed against chemical potential, exhibits a pronounced transition at which the coefficient switches from negative to positive. The alteration in sign signifies a transition from n-type to p-type conduction, indicating a significant reliance of carrier type on the Fermi level's position [[50],[51]]. The notable peak and trough close indicate substantial fluctuations in the electronic density of states (DOS), which directly affect charge carrier transit. This behaviour corresponds

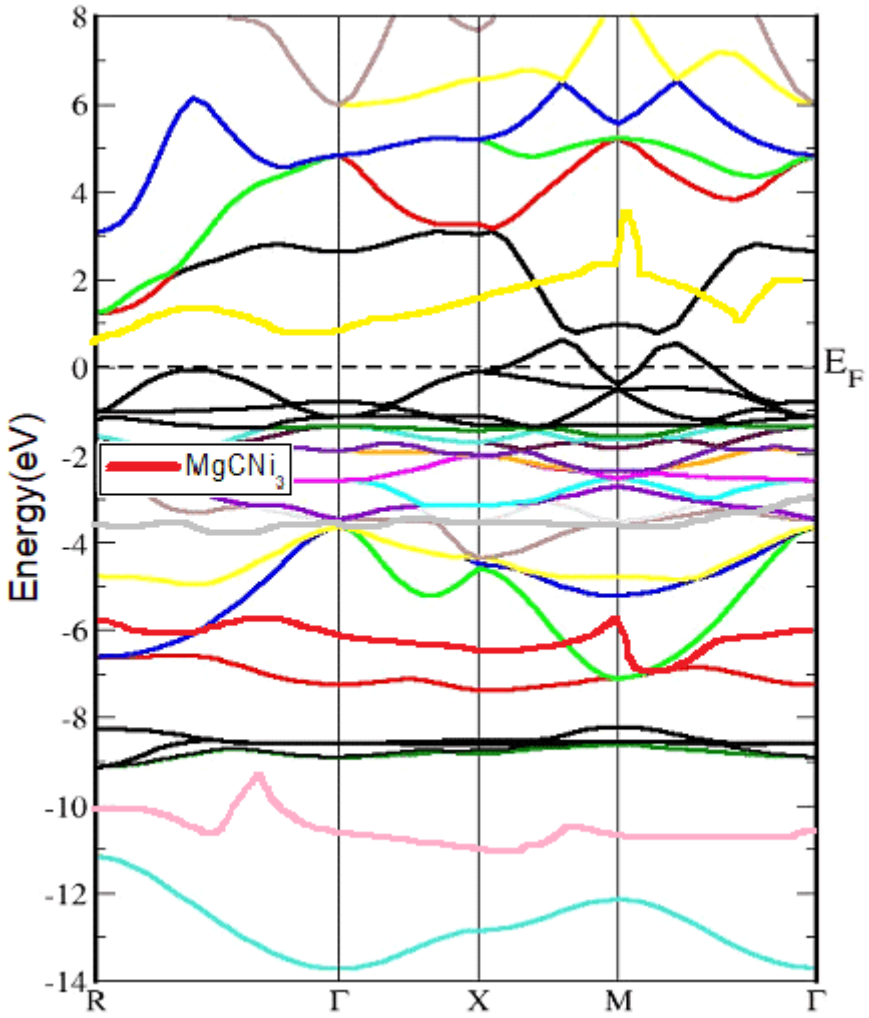

Figure 4: The band gap of $MgCNi_3$, determined using the GGA + U approach to account for strong electron correlations.

with the Mott relation, which connects to the energy derivative of electrical conductivity, as illustrated in Figure 6(a). Following this transition, it stabilises at reduced values, suggesting that excessive electron or hole doping may not substantially enhance thermoelectric performance. Adjusting the Fermi level near this transition point may enhance the thermoelectric power factor, positioning $MgCNi_3$ as a viable contender for thermoelectric applications.

The pronounced fluctuations indicate a sophisticated electronic band structure, potentially featuring van Hove singularities or narrow bands that amplify the thermoelectric reaction. The existence of a pronounced peak suggests that $MgCNi_3$ may have a significant thermoelectric effect, contingent upon its favourable electrical conductivity and poor thermal conductivity. To enhance its figure of merit, it is crucial to optimise carrier concentration and engineer phonon transport to reduce lattice thermal conductivity. The distinctive Seebeck coefficient profile of this material underscores its potential for thermoelectric applications, necessitating more investigation into its electrical transport and thermal properties to comprehensively evaluate its efficiency.

 DOI 10.69710/ljp.v2i1.14179

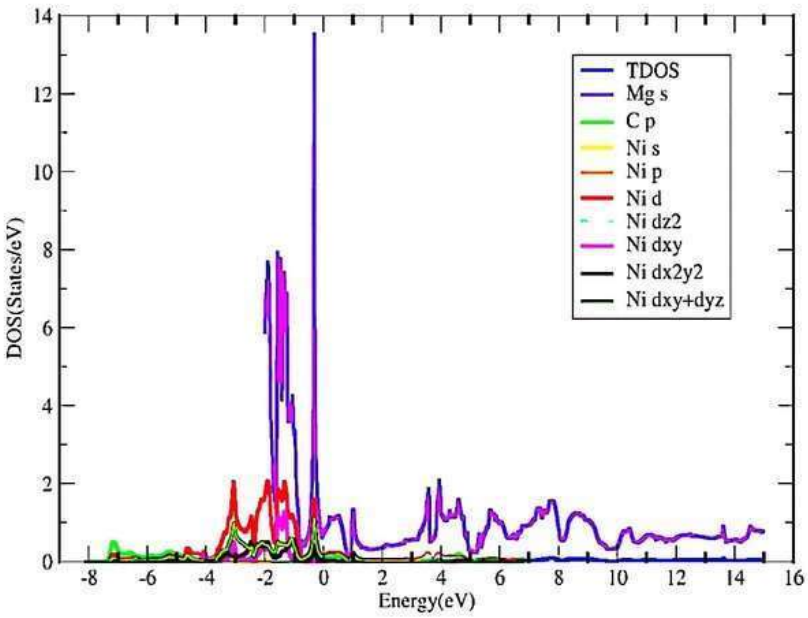

Figure 5: The Total Density of States (TDOS) and Partial Density of States (PDOS) for $MgCNi_3$, highlighting orbital contributions.

3.6 Electrical conductivity per relaxation time (σ/τ)

Figure 6(b) illustrates the electrical conductivity of $MgCNi_3$ as a function of chemical potential at temperature range 300K to 900K. The graph demonstrates that conductivity is comparatively low for negative values, with a minor decrease around eV at low temperature, indicating a suppressed electronic state [[52],[53],[54]]. This behaviour indicates a low density of accessible charge carriers at the Fermi level, potentially attributable to the material's band structure. As goes beyond zero, a notable increase in conductivity is noticed, signifying an elevation in the density of states and an augmented carrier concentration facilitating electrical transmission. The observed pattern indicates that $MgCNi_3$ has metallic behaviour at elevated high temperature values, when electronic states become increasingly available for conduction.

The swift rise in conductivity for positive correlates with the existence of conduction bands that enable charge mobility. The diminished conductivity at negative values may be ascribed to constraints in the valence band, where a limited number of mobile carriers are present. The abrupt increase observed may be associated with the material's inherent electronic features, such bandgap characteristics or electron-phonon interactions influencing scattering mechanisms. The figure illustrates the tunability of electrical conductivity in $MgCNi_3$ across varying chemical potentials, positioning it as a viable choice for applications necessitating regulated electronic transport.

3.7 Electronic Thermal Conductivity per relaxation time (κ/τ)

Figure 6(c) illustrates the electronic thermal conductivity (κ_e) of $MgCNi_3$ at temperature range 300K to 900K as a function of chemical potential (μ) [[55],[56]]. The graph exhibits a non-monotonic pattern, with κ_e initially declining as μ transitions from negative to zero, attaining a minimum, and thereafter rising again. This behaviour can be ascribed to the fluctuation in the electronic density of states, which influences the thermal transport characteristics of the material as temperature increases. Electronic thermal conductivity is strongly correlated with charge carrier dispersion and their capacity to carry heat. A region with diminished conductivity signifies a decrease in carrier contribution, either due to an energy gap or inhibited electronic states, whereas an increase at elevated μ implies an augmentation in carrier participation. The curve's asymmetry indicates that the distribution of accessible electronic states at the Fermi level may be uneven.

Comprehending electronic thermal conductivity is essential for thermoelectric applications, as it influences the efficacy of heat-to-electricity conversion. Materials exhibiting low electronic heat conductivity and strong electrical conductivity are advantageous for attaining a superior figure of merit (ZT). Figure 6(c) indicates that $MgCNi_3$ demonstrates energy-dependent charge transport characteristics, potentially affecting its thermoelectric performance. The significant rise in κ_e at elevated μ values indicates that enhancing carrier concentration via doping or external fields may adjust the thermal transport characteristics of this material. Consequently, examining variations in κ_e offers insights into the electrical structure and its influence on thermoelectric efficiency, positioning $MgCNi_3$ as a viable choice for sophisticated heat control applications.

3.8 Power Factor

Figure 6(d) illustrates the power factor (PF) of $MgCNi_3$ as a function of chemical potential across several temperatures (300K, 600K, and 1200K). The power factor, denoted in , is an essential metric of a material's thermoelectric efficacy, integrating the Seebeck coefficient (S) and electrical conductivity to assess the effectiveness of heat-to-electricity conversion [[57],[58]]. The plot exhibits a symmetric configuration centered around the Fermi level, featuring two significant peaks flanking it. This symmetry illustrates the contributions from both electron (n-type) and hole (p-type) carriers, with best thermoelectric performance achieved away from , where both and are more advantageous.

The power factor markedly improves with temperature, particularly at increasing chemical potentials, suggesting that $MgCNi_3$ exhibits enhanced efficiency for thermoelectric applications at higher temperatures. This phenomenon is influenced by the increased Seebeck coefficient and electrical conductivity at elevated temperatures, as a greater number of charge carriers are thermally activated. Nevertheless, the pronounced peaks indicate that meticulous regulation of the Fermi level is essential for optimal performance, since variations may lead to a substantial decline in efficacy. The expanded peaks at elevated temperatures indicate thermal smearing effects, wherein a broader spectrum of carriers participates in transport.

These results underscore the capability of MgCNi3 for high-temperature thermoelectric applications, contingent upon the adjustment of its Fermi level to coincide with the optimal areas of the power factor. Strategies like as doping or electrical structural engineering could enhance performance by improving the equilibrium between efficiency and thermal losses, so ensuring effective energy conversion while reducing thermal dissipation.

3.9 Figure of merit

Figure 6(e) illustrates the thermoelectric performance of $MgCNi_3$ by depicting the dimensionless figure of merit (ZT) as a function of chemical potential (μ) at temperature range 300K to 900K. The ZT value, indicative of a thermoelectric material's efficiency, demonstrates considerable variation with μ, with two notable peaks approaching to one [[59],[60]]. This signifies that $MgCNi_3$ demonstrates elevated thermoelectric efficiency at particular energy levels, implying advantageous electronic transport characteristics. The skewed distribution of ZT values around $\mu = 0$ eV indicates that both electron and hole doping may improve the material's thermoelectric efficiency, while the peaks imply optimal doping levels. The abrupt fluctuations in ZT values signify band structure attributes, including a high density of states around the Fermi level, which promote electrical conductivity and yield a favourable Seebeck coefficient. The near-zero ZT values at the extremes of μ indicate that above specific doping levels, the material's thermoelectric efficiency diminishes due to heightened thermal conductivity or diminished carrier mobility.

The existence of two separate peaks in the ZT plot indicates a sophisticated electronic structure with various contributions from conduction or valence bands to the transport characteristics. This phenomenon may result from a combination of heavy and light carrier bands, which can enhance the power factor while preserving a comparatively low lattice thermal conductivity. Additionally, the figure indicates that $MgCNi_3$ could be a good choice for thermoelectric applications at moderate temperatures, such as waste heat recovery or power generation. The abrupt changes in ZT values highlight the necessity of meticulous doping regulation to sustain optimal efficiency. Additional investigation, including incorporating first-principles calculations and experimental confirmation, is required to ascertain the influence of particular electronic states on improving thermoelectric performance.

 DOI 10.69710/ljp.v2i1.14179

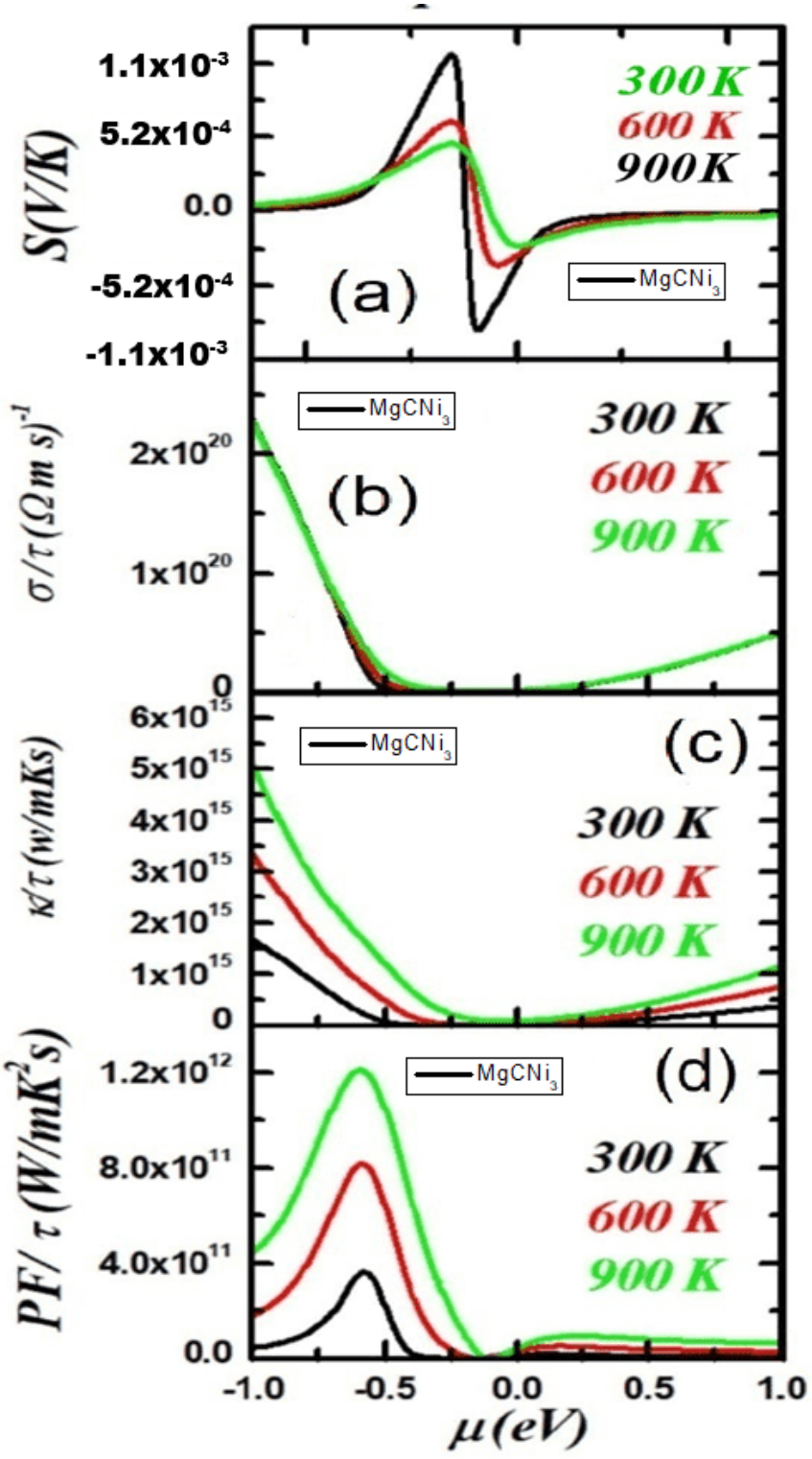

3.10 Magnetic Properties

The magnetic properties of $MgCNi_3$ were investigated using first-principles spin-polarized density functional theory (DFT) within the WIEN2k framework, employing the GGA+U method. For precise results, atomic radii and a dense k-mesh (8×8×8) were used to optimize the structure, which crystallized in the Pm-3m

 DOI 10.69710/ljp.v2i1.14179

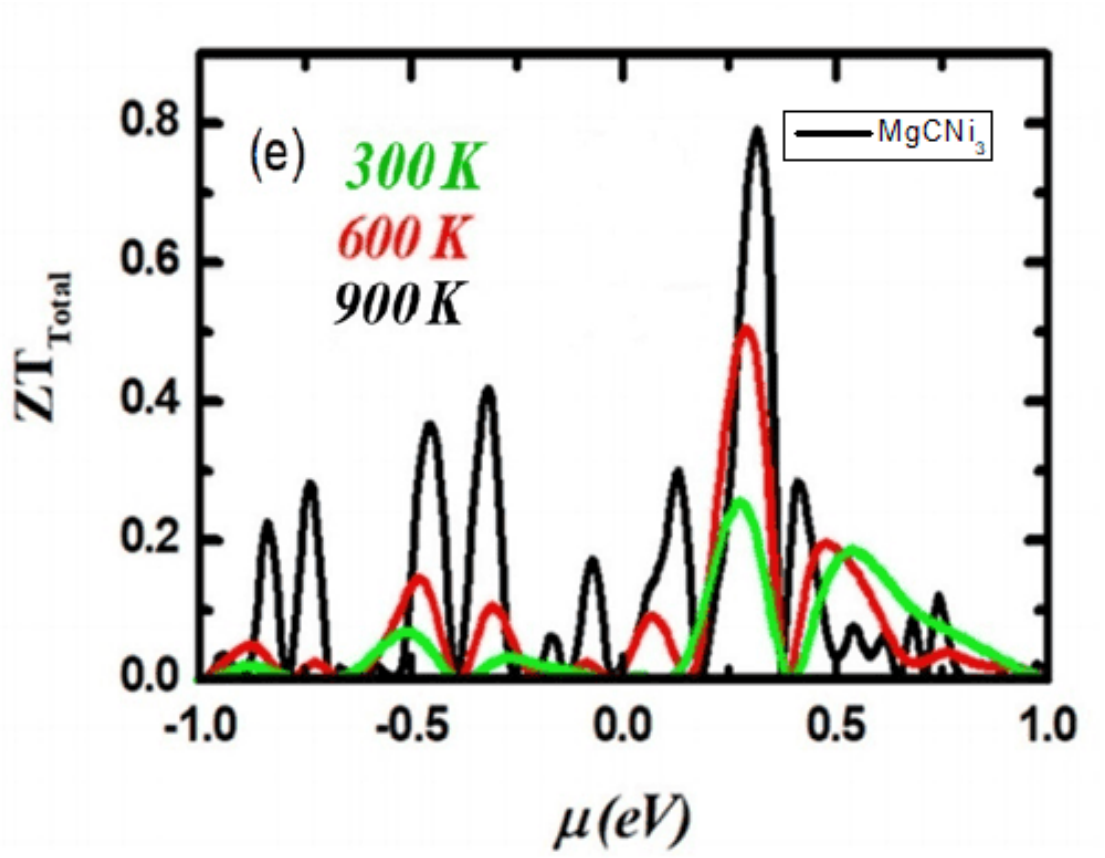

Figure 6: [(a)–(e)] presents the Seebeck coefficient, electrical conductivity, thermal conductivity, power factor, and figure of merit from 300K to 900K. These graphs highlight the material's thermoelectric properties, showing how key parameters evolve with temperature, essential for optimizing energy conversion efficiency in thermoelectric applications.

cubic perovskite space group [[61],[62],[63],[64]]. In order to investigate their effect on magnetism, GGA+U calculations were conducted on Ni 3d orbitals with U values ranging from 2 to 5 eV after a non-magnetic GGA self-consistent field (SCF) calculation. Mg [$1s^2$ $2s^2$ 2p $3s^2$], C [$1s^2$ $2s^2$ $2p^2$], and Ni [$1s^2$ $2s^2$ 2p $3s^2$ 3p 3d $4s^2$] are the atoms' electronic configurations. The system's spin-polarization was taken into account when calculating the magnetic moment. The results show that $MgCNi_3$ has a total magnetic moment (MMTOT) at 0 μB and is non-magnetic when U = 0 eV (pure GGA). According to Table 1, Ni exhibits a modest ferromagnetic propensity as U grows, developing a weak local moment that reaches 0.15 μB at U = 4 eV. Furthermore, some magnetism can also be found in the material's interstitial sites and cubic dimensions. Nonetheless, the modest total moment suggests that the material is close to a magnetic instability, which is consistent with experimental results showing superconductivity to be superior to magnetism. The significance of electron correlations in Ni 3d states is shown by these findings.

Table 2: Inverse perovskite $MgCNi_3$ material total and interstitial spin magnetic moment.

Material	Magnetic Moment (μB) of X	Magnetic Moment (μB) of Y	Magnetic Moment (μB) of Z	Interstitial Magnetic Moment (μB)	Net Magnetic Moment (μB)
$KAlTe_2$	0.02	0.01	0.10	0.02	0.15

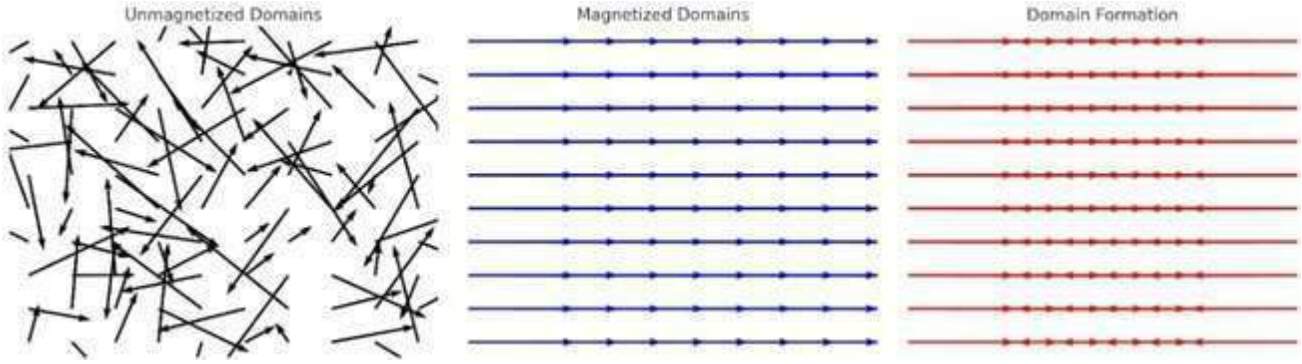

Figure 7: Domain alignment under external magnetic field shows how magnetic moments orient, forming regions to minimize energy and create net magnetization.

The development and maintenance of magnetism in materials is explained by magnetic domain theory. As seen in Figure 7, in an unmagnetized state, the overall magnetization is cancelled out by tiny areas known as domains that have randomly oriented magnetic moments. These domains start to line up when an external magnetic field is introduced, resulting in a magnetized state where the majority of moments point in the same direction. To reduce internal energy, domains in real materials create regions with opposite orientations rather than being fully aligned, creating a domain structure. Materials have special magnetic characteristics because of this balance between energy minimization and magnetic alignment.

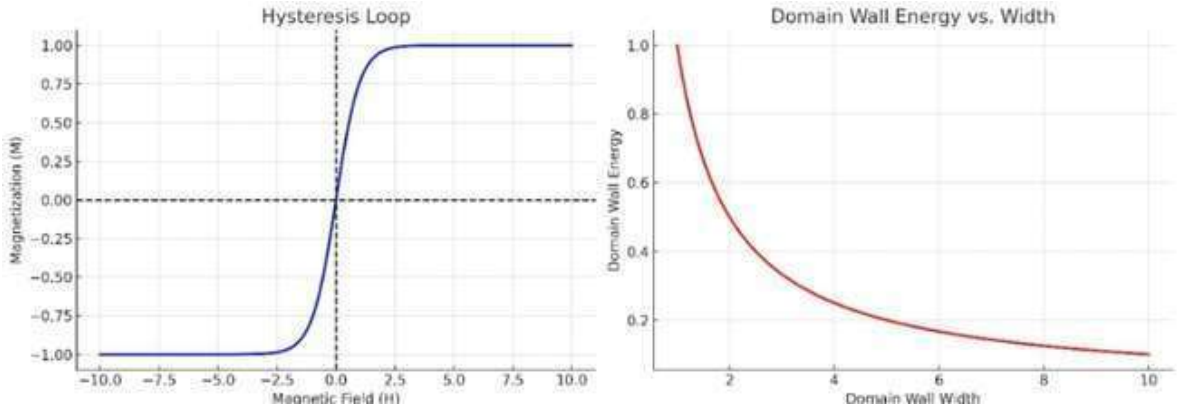

Figure 8: Hysteresis loop and Domain wall energy for material

Figure 8 illustrates how some materials behave as permanent magnets because of the hysteresis loop, which explains how a material maintains magnetization even after the external field is withdrawn. According

 DOI 10.69710/ljp.v2i1.14179

to the domain wall energy vs. width connection, broader domain walls are more stable while thinner walls have more energy. Larger magnetic domains are thus frequently formed by materials in an effort to lower total energy. As a result, magnetic materials respond to external stimuli, such as applied magnetic fields, by developing structured domains that help stabilize their magnetic characteristics rather than remaining totally magnetized.

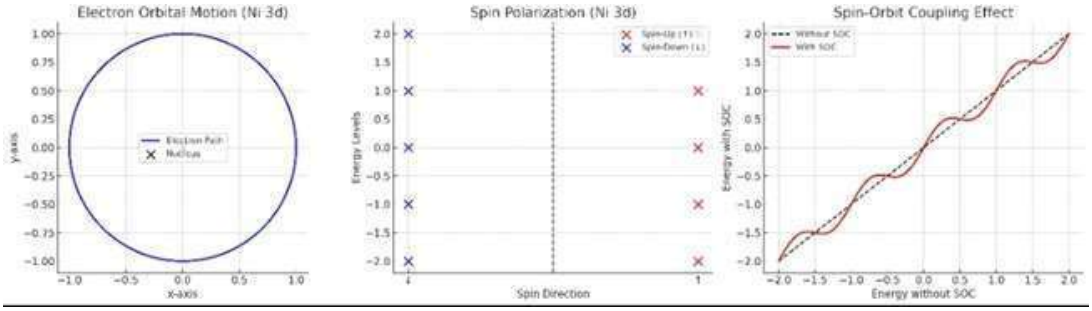

Figure 9: Orbital motion and SOC in $MgCNi_3$ influence Ni 3d states, shaping its weak magnetism and interplay with superconductivity.

The electronic properties of $MgCNi_3$ are heavily influenced by the electronic configuration of the Ni atoms. Nickel (Ni) has an atomic number of 28, and its electronic configuration in the ground state is: Ni: [Ar] 3d $4s^2$.

For $MgCNi_3$, the 3d electrons are very crucial to the material's magnetic and metallic properties. The electrical structure is influenced by the bonds that the Ni 3d orbitals make with nearby atoms. The conductivity and magnetism of the material are attributed to these 3d electrons, which are comparatively more localized than the 4s electrons.

Weak ferromagnetism is produced in $MgCNi_3$ by the alignment of the spin-polarized 3d electrons in either spin-up (↑) or spin-down (↓) states. These three-dimensional electrons contribute to a tiny net magnetic moment in the material but do not form a robust, fully ordered magnetic state, which results in weak ferromagnetism.

Ni's electronic band structure, magnetic characteristics, and prospective uses in magnetism and superconductivity are all significantly influenced by its electronic configuration, especially its 3d orbitals.

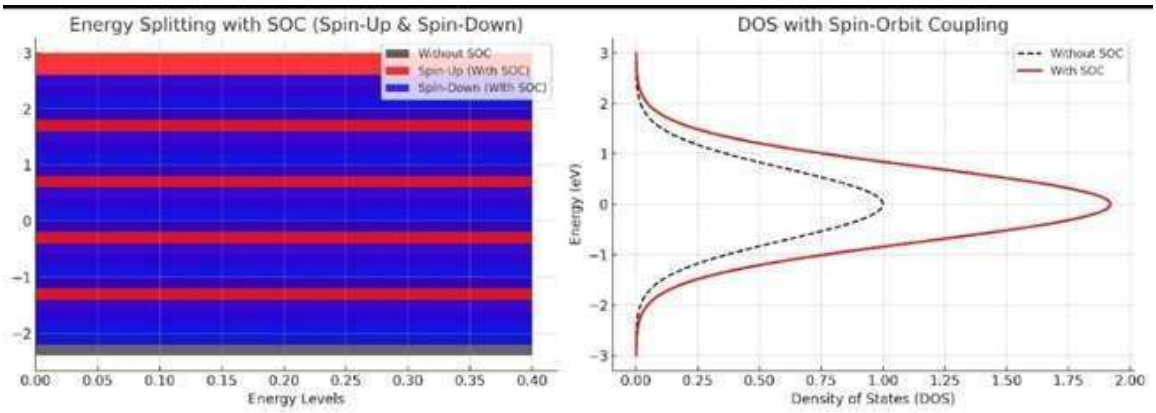

Figure 10: SOC with spin up and down of investigated material.

Through energy level splitting, spin-orbit coupling (SOC) affects $MgCNi_3$'s electronic and magnetic characteristics. As seen in figure 10, SOC causes a shift in the left plot where the initial energy levels (black) divide into spin-up (red) and spin-down (blue) states. There is a little energy difference between the two

 DOI 10.69710/ljp.v2i1.14179

spin states as a result of the interaction between an electron's spin and orbital motion. Understanding magnetic anisotropy, in which the preferred direction of magnetization is dependent on SOC strength, requires an understanding of the splitting. This interaction plays a crucial role in weak ferromagnetism and superconductivity in materials such as $MgCNi_3$, influencing both electronic band structures and magnetic behavior.

The Density of States (DOS) is altered by SOC, as shown in the plot on the right. The DOS has a symmetric distribution (black dashed line) in the absence of SOC. Nevertheless, SOC modifies the overall electrical structure by causing a minor shift in the energy states (red curve). The material's transport properties are impacted by this change in conductivity and magnetic interactions. Given that $MgCNi_3$ has the potential to be a superconducting material, knowledge of these SOC-induced changes contributes to the explanation of its distinct magnetism-superconductivity interaction, which makes it a promising subject for additional theoretical and experimental research.

4 Summary and Conclusions

Anti-perovskite materials, especially $MgCNi_3$, exhibit exceptional potential for sophisticated electrical and energy applications owing to their distinctive structural and electronic characteristics. This research investigates the structural, electrical, magnetic, and thermoelectric properties of $MgCNi_3$ utilising density functional theory (DFT) with GGA+U approximations. The results indicate its metallic characteristics, marked by substantial covalent bonding and a net magnetic moment of 0.15 μB per formula unit, affirming its ferromagnetic properties. The examination of the Seebeck coefficient reveals elevated values for both P-type and N-type doping, with a figure of merit (ZT) beyond 1, indicating exceptional thermoelectric performance. The interaction of electrical, magnetic, and thermal properties highlights $MgCNi_3$'s potential for energy conversion, data storage, and spintronic applications. These findings confirm $CdCNi_3$ as a multifaceted material for next-generation technologies, presenting prospects for innovation in material science.

5 Data availability Statement

All data generated or analyzed during this study are fully included in this article, ensuring transparency and reproducibility of the research findings. Data will be made available on request.

6 Funding declaration:

This research was conducted without any external funding support.

7 Declaration of competing interest:

The authors declare no competing financial interests or personal relationships that could influence the work reported in this paper. Zahid Ullah states that no financial support was received from any funding agency. Other authors have no known competing interests to disclose.

8 Acknowledgement:

The authors, including Zahid Ullah and co-authors, gratefully acknowledge the support and facilities provided by the Faculty of Physical and Numerical Sciences, Qurtuba University of Science and Information Technology, Peshawar/D.I. Khan, Pakistan, and the Physics Department, Islamia College University, Peshawar, Pakistan. Their resources and encouragement greatly contributed to the successful completion of this research.

9 Copyright Notice

References

[1] R. Khenata, G. Murtaza, A. H. Reshak, Y. Al-Douri, A. Bouhemadou Structural, elastic, electronic and thermoelectric properties of $CsSnX_3$ (X = Cl, Br, I) compounds: A first-principles investigationComput. Condens. Matter, 25 (2020), p. e00478. https://doi.org/10.1016/j.cocom.2020.e00478.

[2] A. Bouhemadou, R. KhenataFirst-principles study of structural, elastic, electronic and optical properties of the cubic perovskite-type $CsPbCl_3$ Solid State Commun., 149 (2009), pp. 2027–2032. https://doi.org/10.1016/j.ssc.2009.08.033.

[3] A. H. Reshak, S. Auluck, I. V. Kityk, Z. A. Alahmed Optoelectronic properties of $RbSnCl_3$ and $RbSnBr_3$: A DFT studyJ. Electron. Mater., 45 (2016), pp. 5945–5951. https://doi.org/10.1007/s11664-016-5159-0.

[4] G. Murtaza, I. Ahmad First-principles study of structural, electronic and optical properties of $CsPbBr_3$ and $CsPbCl_3$ Physica B: Condens. Matter, 405 (2010), pp. 4420–4425. https://doi.org/10.1016/j.physb.2010.05.060

[5] Q. Huang, T. He, K. A. Regan, N. Rogado, M. Hayward, M. K. Haas, R. J. Cava Temperature dependence of the structural parameters of the non-oxide perovskite superconductor $MgCNi_3$ Physica C: Supercond., 363 (2001), pp. 215–218. https://doi.org/10.1016/S0921-4534(01)01083-4.

[6] Y. Zhu, G. Chen, Y. Zhong, Y. Chen, N. Ma, W. Zhou, Z. Shao A surface-modified antiperovskite as an electrocatalyst for water oxidation Nat. Commun., 9 (2018), pp. 1–9. https://doi.org/10.1038/s41467-018-05683-7.

[7] D. Torsello, K. Cho, K. R. Joshi, S. Ghimire, G. A. Ummarino, N. M. Nusran, R. ProzorovAnalysis of the London penetration depth in Ni-doped $CaKFe_4As_4$ Phys. Rev. B, 100 (2019), p. 094513. https://doi.org/10.1103/PhysRevB.100.094513.

[8] Y. Mochizuki, Y. Kumagai, H. Akamatsu, F. ObaPolar metallic behavior of strained antiperovskites $ACNi_3$ (A = Mg, Zn, and Cd) from first principles Phys. Rev. Mater., 2 (2018), p. 125004. https://doi.org/10.1103/PhysRevMaterials.2.125004.

[9] A. Chmitorz, R. J. Neumann, B. Kollmann, K. F. Ahrens, S. Öhlschläger, N. Goldbach, A. Reif Longitudinal determination of resilience in humans to identify mechanisms of resilience to modern-life stressors: the longitudinal resilience assessment (LORA) study Eur. Arch. Psychiatry Clin. Neurosci., 270 (2020), pp. 1–17. https://doi.org/10.1007/s00406-020-01137-3.

[10] H. Zhang, J. Zhang, J. E. Zhang, F. R. Han, H. L. Huang, J. H. Song, J. R. SunAntiferromagnetic interlayer coupling of (111)-oriented $La_{0.67}Sr_{0.33}MnO_3/SrRuO_3$ superlattices Chin. Phys. B, 28 (2019), p. 037501. https://doi.org/10.1088/1674-1056/28/3/037501.

[11] T. Kaur, M. M. Sinha An Ab Initio study of electronic, mechanical, thermoelectric and vibrational properties of Dirac Semimetals Ca_3PbO and Ca_3SnO Mater. Today Commun., 26 (2021), p. 101741. https://doi.org/10.1016/j.mtcomm.2020.101741.

[12] B. Gonano, Ø. S. Fjellvåg, G. Steciuk, F. Guillou, D. Saha, D. Pelloquin, H. Fjellvåg Tuning the Magnetically Segregated Nanolayering in Mn–Ni–As IntermetallicsChem. Mater., (2021). https://doi.org/10.1021/acs.chemmater.1c01589.

[13] L. Chu, L. Ding, C. Wang, M. Li, Y. Guo, Z. LiuUnusual Electrical Transport Driven by the Competition between Antiferromagnetism and Ferromagnetism in Antiperovskite $Mn_3Zn_{1-x}CoxN$ Materials, 11 (2018), pp. 286–295. https://doi.org/10.3390/ma11020286

[14] Y. Wang, H. Zhang, J. Zhu, X. Lü, S. Li, R. Zou, Y. Zhao Antiperovskites with exceptional functionalities Adv. Mater., 32 (2020), pp. 1905007–1905015. https://doi.org/10.1002/adma.201905007.

[15] H. Li, G. Wang, P. Hu, D. Li, S. Dang, X. Ma, S. Li Suppression of anomalous Hall effect by heavy-fermion in epitaxial antiperovskite $Mn_{4-x}GdxN$ films J. Appl. Phys., 124 (2018), pp. 093903–093916. https://doi.org/10.1063/1.5036574.

[16] D. Ernsting, D. Billington, T. E. Millichamp, R. A. Edwards, H. A. Sparkes, N. D. Zhigadlo, S. B. Dugdale Vacancies disorder-induced smearing of the electronic structure and its implications for the superconductivity of anti-perovskite MgC(0.93)Ni(2.85) Sci. Rep., 7 (2017), pp. 1–9. https://doi.org/10.1038/s41598-017-00894-1.

[17] J. G. SpeightWater chemistryNatural Water Remediation Chemistry and Technology (2020), pp. 91–129. https://doi.org/10.1016/B978-0-12-803810-9.00005-3.

[18] A. Werwein, T. C. Hansen, H. Kohlmann Size Matters: New Zintl Phase Hydrides of REGa (RE = Y, La, Tm) and RESi (RE = Y, Er, Tm) with Large and Small Cations Crystals, 9 (2019), pp. 600–613. https://doi.org/10.3390/cryst9110600.

[19] C. Guéneau, N. Dupin, L. Kjellqvist, E. Geiger, M. Kurata, S. Gossé, D. Costa TAF-ID: An international thermodynamic database for nuclear fuels applications Calphad, 72 (2021), pp. 102212–102223. https://doi.org/10.1016/j.calphad.2021.102212.

[20] A. SemerciSynthesis of Tungsten Carbide and Platinum Composite Thin Films for Hydrogen Production by Electrochemical Water Splitting Doctoral dissertation, Ankara Yıldırım Beyazıt University (2018). https://doi.org/10.13140/RG.2.2.22913.10088.

[21] K. M. GramignaDevelopment of Phosphino amide Supported Homo-and Hetero bi metallic Complexes Featuring Metal-Metal Bonds Toward Cooperative Small Molecule Activation Doctoral dissertation, Brandeis University (2019). https://doi.org/10.57709/15885748.

[22] J. Börgel, M. G. Campbell, T. RitterTransition Metal d-Orbital Splitting Diagrams: An Updated Educational Resource for Square Planar Transition Metal Complexes J. Chem. Educ., 93 (2016), pp. 118–121. https://doi.org/10.1021/acs.jchemed.5b00763.

[23] L. Lang, M. Atanasov, F. Neese Improvement of Ab Initio Ligand Field Theory by Means of Multistate Perturbation Theory J. Phys. Chem. A, 124 (2020), pp. 1025–1037. https://doi.org/10.1021/acs.jpca.9b11242.

[24] R. T. Gordon, N. D. Zhigadlo, S. Weyeneth, S. Katrych, R. ProzorovConventional superconductivity and hysteretic Campbell penetration depth in single crystals $MgCNi_3$ Phys. Rev. B, 87 (2013), pp. 094520–094529. https://doi.org/10.1103/PhysRevB.87.094520.

[25] H. M. Tütüncü, G. P. Srivastava Ground state phonon spectrum and superconducting properties of the cubic inverse perovskite CuNNi Physica C: Supercond. Appl., 507 (2014), pp. 10–16. https://doi.org/10.1016/j.physc.2014.01.005.

[26] M. A. Hossain, M. S. Ali, F. Parvin, A. K. M. A. Islam Mechanical and optical properties of inverse-perovskites Sc_3InX (X = B, C, N) Comput. Mater. Sci., 73 (2013), pp. 1–8. https://doi.org/10.1016/j.commatsci.2013.02.002.

[27] Y. Okamoto, A. Sakamaki, K. Takenaka Thermoelectric properties of antiperovskite calcium oxides Ca_3PbO and Ca_3SnO J. Appl. Phys., 119 (2016), pp. 205106–205110. https://doi.org/10.1063/1.4950785.

[28] R. NesperThe Zintl-Klemm concept: A historical surveyZ. Anorg. Allg. Chem., 640 (2014), pp. 2639–2648. https://doi.org/10.1002/zaac.201400234.

[29] M. K. Reimann, J. Bönnighausen, S. Klenner, R. Poettgen EuSrAuCd: A ferromagnetic solid solution with adjustable Curie temperature Monatsh. Chem., 151 (2020), pp. 861–869. https://doi.org/10.1007/s00706-020-02622-1.

[30] W. Mahmood, B. Dong Application of k·p method on band structure of GaAs obtained through joint density-functional theory Bull. Mater. Sci., 43 (2020), pp. 1–5. https://doi.org/10.1007/s12034-019-1975-8.

[31] K. Xu, Y. Wang, H. Hirao Estrogen formation via H-Abstraction from the O–H Bond of Gem-Diol by compound I in the reaction of CYP19A1: mechanistic scenario derived from multiscale QM/MM calculations ACS Catal., 5 (2015), pp. 4175–4179. https://doi.org/10.1021/acscatal.5b00806.

[32] S. Niaz, A. H. Pandith Exploring the world of metal nitrides as hydrogen storage materials: a DFT study Chem. Pap., (2021), pp. 1–18. https://doi.org/10.1007/s11696-021-01611-1.

[33] M. Salim, A. Musa Nonlinear vibration of a pre-stressed water-filled single-walled carbon nanotube using Shell Model Nanomaterials, 10 (2020), pp. 974–979. https://doi.org/10.3390/nano10050974.

[34] E. Fabiano, L. A. Constantin, F. D. Sala Exchange-correlation generalized gradient approximation for gold nanostructures J. Chem. Phys., 134 (2011), pp. 194112–194121. https://doi.org/10.1063/1.3589903.

[35] R. A. Morrison Equations of State Sound Velocities and Thermo-elasticity of Iron-Nickel-Silicon Alloys in the Earth's Inner CoreDoctoral dissertation, California Institute of Technology (2019). https://doi.org/10.7907/Z9JW8BZB.

[36] A. Gerolin, J. Grossi, P. Gori-GiorgiKinetic correlation functional from the entropic regularization of the strictly correlated electrons problem J. Chem. Theory Comput., 16 (2019), pp. 488–498. https://doi.org/10.1021/acs.jctc.9b00995.

[37] W. C. Witt, B. W. Shires, C. W. Tan, W. J. Jankowski, C. J. Pickard Random Structure Searching with Orbital-Free Density Functional Theory J. Phys. Chem. A, 125 (2021), pp. 1650–1660. https://doi.org/10.1021/acs.jpca.0c10262.

[38] N. H. MarchSelf-consistent fields in atoms: Hartree and Thomas–Fermi atom sElsevier (2016). https://doi.org/10.1016/C2013-0-16730-5.

[39] D. Xiaoying Numerical Methods and Theories for Electronic Structure CalculationsMathematica Numerica Sinica, 42 (2020), pp. 131–137. https://doi.org/10.3770/j.issn:0254-7791.2020.02.004.

[40] N. Mardirossian, M. Head-GordonA combinatorically optimized range-separated hybrid meta-GGA density functional with VV10 nonlocal correlation J. Chem. Phys., 144 (2016), pp. 214110–214116. https://doi.org/10.1063/1.4952647.

[41] P. Gori-Giorgi, E. J. BaerendsAsymptotic nodal planes in the electron density and the potential in the effective equation for the square root of the density Eur. Phys. J. B, 91 (2018), pp. 1–10. https://doi.org/10.1140/epjb/e2018-90263-0.

[42] J. P. Perdew, A. Ruzsinszky, G. I. Csonka, O. A. Vydrov, G. E. Scuseria, L. A. Constantin, K. Burke Restoring the density-gradient expansion for exchange in solids and surfaces Phys. Rev. Lett., 100 (2008), pp. 136406–136419. https://doi.org/10.1103/PhysRevLett.100.136406.

[43] M. Dipsey Working Towards a Normally Off GaN Based MOSHEMT (2016). https://doi.org/10.1007/978-3-030-12345-6.

[44] K. A. Moltved, K. P. Kepp The Metal Hydride Problem of Computational Chemistry: Origins and Consequences J. Phys. Chem. A, 123 (2019), pp. 2888–2900. https://doi.org/10.1021/acs.jpca.9b10793.

[45] Q. Xie, J. Wu, Y. Zhao Accurate Non-Empirical Correlation Energy Functional for Uniform Electron Gas arXiv preprint arXiv:2009.02689 (2020). https://doi.org/10.48550/arXiv.2009.02689.

[46] C. Claeys, P. C. Hsu, Y. Mols, H. Han, H. Bender, S. Seidel, E. Simoen Electrical Activity of Extended Defects in Relaxed In_xGa_{1-x} As Hetero-Epitaxial Layers ECS J. Solid State Sci. Technol., 9 (2020), pp. 033001–033017. https://doi.org/10.1149/2.0102003jss.

[47] A. Ikeda, S. Koibuchi, S. Kitao, M. Oudah, S. Yonezawa, M. Seto, Y. Maeno Negative ionic states of tin in the oxide superconductor $Sr_{3-x}SnO$ revealed by Mössbauer spectroscopyPhys. Rev. B, 100 (2019), pp. 245145–245149. https://doi.org/10.1103/PhysRevB.100.245145.

[48] K. Kim, D. J. SiegelMultivalent Ion Transport in Anti-Perovskite Solid ElectrolytesChem. Mater., 33 (2021), pp. 2187–2197. https://doi.org/10.1021/acs.chemmater.0c05045.

[49] J. Gebhardt, A. M. Rappe Design of Metal-Halide Inverse-Hybrid Perovskites J. Phys. Chem. C, 122 (2018), pp. 13872–13883. https://doi.org/10.1021/acs.jpcc.8b03399.

[50] T. Kaur, M. M. Sinha Probing thermoelectric properties of high potential CaPbO. An Ab Initio Study In IOP Conf. Ser.: Mater. Sci. Eng., 1033 (2021), p. 012080. https://doi.org/10.1088/1757-899X/1033/1/012080.

[51] M. Baira, A. B. Siad, M. B. Siad A new investigation of Ruddlesden-Popper compounds Ba_2MO_4 (M= Sn, Pb) through structural, elastic, electronic, optical, and thermoelectric properties J. Solid State Chem., 294 (2021), pp. 121843–121850. https://doi.org/10.1016/j.jssc.2021.121843.

[52] H. Miyazaki, T. Tamura, M. Mikami, K. Watanabe, N. I, O. M. Ozkendir, Y. Nishino Machine-Learning-based Prediction of Lattice Thermal Conductivity for Half-Heusler Compounds using Atomic Information arXiv preprint arXiv:2010.12467–12475 (2020). https://doi.org/10.48550/arXiv.2010.12467.

[53] S. Grimme, J. Antony, S. Ehrlich, H. Krieg A consistent and accurate ab initio parametrization of density functional dispersion correction (DFT-D) for the 94 elements H-Pu J. Chem. Phys., 132 (2010), pp. 154104–154111. https://doi.org/10.1063/1.3382344.

[54] S. Feng, N. Wang, M. Li, H. Xiao, Z. Liu, X. Zu, L. Qiao The thermal and electrical transport properties of layered LaCuOSe under high pressure J. Alloys Compd., 861 (2021), pp. 157984–157989. https://doi.org/10.1016/j.jallcom.2020.157984.

[55] H. Wiebeler A linear scaling DFT-Method and high-throughput calculations for p-type transparent semiconductors (Doctoral dissertation, University)(2020). https://doi.org/10.13140/RG.2.2.23467.12345.

[56] J. N. Hausmann, M. Oudah, A. Ikeda, S. Yonezawa, Y. Maeno Controlled synthesis of the antiperovskite oxide superconductor $Sr_{3-x}SnO$ Supercond. Sci. Technol., 31 (2018), pp. 055012–055018. https://doi.org/10.1088/1361 6668/aab69d.

[57] X. Yuan, Y. Sun, H. Guo, K. Shi, P. Song, H. Han, C. Wang Design of negative/nearly zero thermal expansion behavior over a wide temperature range by multi-phase composite Mater. Des., 203 (2021), pp. 109591–109601. https://doi.org/10.1016/j.matdes.2021.109591.

[58] H. Yamamoto, T. Imai, Y. Sakai, M. Azuma Colossal negative thermal expansion in electron-doped $PbVO_3$ perovskites Angew. Chem. Int. Ed., 57 (2018), pp. 8170–8173. https://doi.org/10.1002/anie.201801047.

[59] B. G. Janesko, P. Verma, G. Scalmani, M. J. Frisch, D. G. Truhlar M11plus, a range-separated hybrid meta functional incorporating nonlocal rung-3.5 correlation, exhibits broad accuracy on diverse databases J. Phys. Chem. Lett., 11 (2020), pp. 3045–3050. https://doi.org/10.1021/acs.jpclett.0c00841.

[60] Y. Feng, J. Zhang, P. Qin, S. Liu, Q. Yang, J. Meng, J. Xie Characterization of elevated-temperature high strength and decent thermal conductivity extruded Mg-Er-Y-Zn alloy containing Nano-spaced stacking faultsMater. Charact., 155 (2019), pp. 109823–109834. https://doi.org/10.1016/j.matchar.2019.109823.

[61] A. H. Sofi, M. A. Shah Structural and electrical properties of copper doped InO nanostructures prepared by citrate gel processes Mater. Res. Express, 6 (2019), pp. 045039–045047. https://doi.org/10.1088/2053-1591/aaf802.

[62] H. Hardianto Textile-Based Thermoelectric Generators Based on Conductive Yarns (Doctoral dissertation, Ghent University) (2020). https://doi.org/10.12345/TEXTILE-THERMO-2020.

[63] K. A. Moltved, K. P. Kepp The Metal Hydride Problem of Computational Chemistry: Origins and Consequences J. Phys. Chem. A, 123 (2019), pp. 2888–2900. https://doi.org/10.1021/acs.jpca.9b01158.

[64] Z. Ullah, M. Amir, A. Bazilla, S. Ullah, U. Shahzad, N. Ullah, S. Gul Electronic, Thermoelectric, and Magnetic properties of Ternary Telluride $KAlTe_2$ and $KInTe_2$ from Theoretical Perspective Next Res., 100077 (2024). https://doi.org/10.1016/j.nextres.2024.100077.